Enumeration of Not-Yet-Synthesized Zeolitic Zinc Imidazolate MOF Networks: A Topological and DFT Approach

I. A. Baburin,[†] S. Leoni,*[,‡] and G. Seifert[§]

Samara State University, Ac. Pavlov St. 1, 443011 Samara, Russia, Max Planck Institut für Chemische Physik fester Stoffe, Nöthnitzer Strasse 40, 01187 Dresden, Germany, and Technische Universität Dresden, Institut für Physikalische Chemie and Elektrochemie, Mommsenstr. 13, 01062 Dresden, Germany

Received: February 26, 2008; Revised Manuscript Received: May 6, 2008

Twenty-one zeolitic imidazolate metal−organic frameworks based on Zn connectors (ZIFs) are derived and compared to known imidazolate networks. Not-yet-synthesized zinc imidazolates are identified on the basis of DFT total energy scoring. The structure with lowest energy is not porous and represents an unusual structure type with **zni** topology. Total energy scoring indicates the **lcs** and **pcb** networks as reliable ZIF candidates. The intrinsic channel chirality of the **lcs** network makes this rare topology an attractive target for the synthetic effort. Among the porous ZIFs candidates, the sodalite type, **sod**, is also found.

Introduction

Microporous zeolite materials have found large use in high-impact technological applications, like petrochemical cracking, water purification and softening, and gas exchange and storage.[1–6] This broad spectrum of applications reflects an impressive framework diversity resulting from reconnecting $Si(Al)O_4$ tetrahedral units. Recently, the attention has turned to metal−organic frameworks (MOFs) as an attractive way of combining this structural diversity with embedded metallic functions to work as catalytic centers.[7] The zeolitic structural manifold is on the contrary very contracted in tetrahedral MOFs. The variety of MOF tetrahedral topologies can in fact be summarized in a few topological representatives. Nonetheless, a promising way of combining high porosity, framework diversity, and transition metal catalytic centers is represented by imidazole-based MOF (IMOF), in particular, with Zn or Co as connectors.[7] IMOFs are in fact expected to allow for a manifold of frameworks due to their structural analogy to silicas. The latter is based on four-coordinated metal (M) centers, close Si−O−Si and M−IM−M angles (IM = imidazolate) and robust M−N bonds (directed bonds). For zinc imidazolates (ZIFs), while the experimental, solvent free, thermodynamically stable compound is very compact and thus basically not porous, some silica-like open frameworks have been synthesized with porous networks (zeolites DFT, GIS, MER) and untypical topologies. This hints at a hidden structural diversity that awaits to be unfolded. Many silicate networks, for example, are only a few kilojoules per mole apart, in terms of bond energy, and the network diversity is due to a judicious choice of synthetic strategies in terms of structure-directing reagents.

The computational approaches to MOFs based on different numerical methods have in general been focused on specific aspects (solvent absorption, phonon spectra, force field design) for some *given* MOFs. Most theoretical studies are concerned with the calculation of properties like electronic structure, mechanical and adsorption properties, and force field engineering for a particular crystal structure.[8,9] The effect of substituting metals or linkers keeping the topology of the crystal structure is only beginning to be considered,[10] and the question of the relationship between metals and ligands (linkers) in terms of bonding characterization and consequences on physical properties, is largely disregarded. Clearly, there is a close relationship between geometry, topology, and physical properties, which does emerge by inspecting correlations between known quantities. In MOFs, the interconnection between topology, porosity, and degree of network interpenetration represents a paradigm for internal surface maximization toward property optimization.[11]

In order to contrast empirical regularities with computational results based on quantitatively reliable methods, we have concentrated on ZIFs because of their extensive polymorphism. The solvent-free zinc imidazolate can be prepared in a straightforward manner by reacting zinc acetylacetonate in a melt of imidazole and tetramethylimidazole.[12] Its structure shows an unprecedented topology (**zni**; hereafter, three-letter bold symbols are used to designate framework types; see http://rcsr.anu.edu.au/) that, up to now, has been observed only in isomorphous $Zn(imid)_2$ and $Co(imid)_2$. The compound is quite dense and allows for narrow channels, making it essentially nonporous. Nonetheless, for the composition $Zn(imid)_2$, several polymorphs were reported from nonconventional synthesis approaches, including some common zeolite topologies (zeolites DFT, BCT, GIS, MER).[7] The latter are porous and show an exceptional chemical stability in refluxing organic solvents and even water. For MOF imidazolates, the catalogue of shapes already known from zeolite atlases or obtained by *ab initio* topological enumerations represents thus a collection of prototypes for new compounds. Clearly, *which one* among them can be synthesized and *which properties* can be expected remains an open issue. Nonetheless, predictions on likely structural realizations are within reach of state-of-art numerical methods. Like it is the case for silica, the paradigm of highest symmetry does not hold in predicting new polymorphs, due to some peculiarities in the angle distributions, which is reflected in lower symmetries for quartz or cristobalite. This calls for the introduction of energetic criteria able to provide a reliable score.

In this work, we focus on the relationships between geometry, topology, network porosity, and total energy. We develop a

* Corresponding author. E-mail: leoni@cpfs.mpg.de.
[†] Samara State University.
[‡] Max Planck Institut für Chemische Physik fester Stoffe.
[§] Technische Universität Dresden.

10.1021/jp801681w CCC: $40.75
Published on Web 07/15/2008

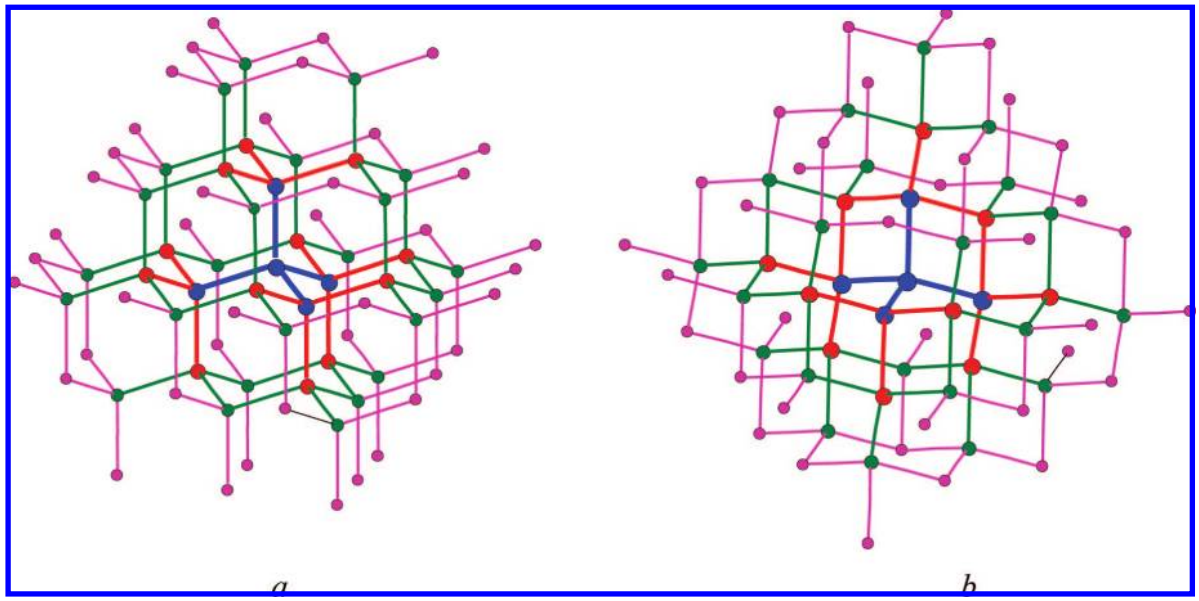

Figure 1. Diamond (a) and $SrAl_2$ (b) structure types. Different colors distinguish the first four coordination spheres. The two nets are different from the second coordination sphere on.

catalogue of shapes based on topological reasoning and augment it by total energy calculations based on DFT. Topology is used as a means to incorporate chemical understanding into an otherwise prohibitively complex free energy scan. In fact, the requirement of local tetrahedral geometry imposes restrictions on the networks which can be formed. Its number remains in principle infinite but countable. The discreteness of the chemical enumeration as it results from including topology is coupled with first principles methods to properly account for many-body factors. Since the reaction products are typically kinetically driven, and depend on as many factors such as ionic strength, temperature, pressure, and polarity of the solvent,[4] our approach is intended as guideline for synthetic diversity toward intelligent synthesis planning.

Computational Details. The construction of ZIF network candidates can be made systematic by means of topology. Under conservation of local Zn tetrahedral coordination, global topological changes were incorporated. This was implemented in variations in second and subsequent coordination shells, or in ring size changes, influencing framework openness and porosity in a systematic way. ZIFs having 3-, 4-, 5-, and 6-membered rings as the shortest ones were constructed. Here, we follow the definition of a ring[13] as the shortest cycle of metal atoms connected by linkers that is not a sum of two cycles of smaller size. The size of a ring is equal to the number of metal atoms (or ligands) in it. For instance, the adamantane cage in the diamond network is bound by four 6-rings, as the shortest loops in the structure. Consider, as an example, diamond (**dia**) and $SrAl_2$ (**sra**) structure types. Both types are identical within the first coordination sphere but differ already in the second coordination shell (Figure 1).

This approach corresponds to a topological sampling of configurational space, from simpler, common structure types, to more involved structural motifs. Proceeding from simplest structure representatives ensures a systematic scan, which is progressive in the complexity and complete in the enumeration. As a measure of this complexity, appropriate topological parameters, like genus or topological density, are useful. In connection with experiments, this may represent a blueprint for MOF network diversity.

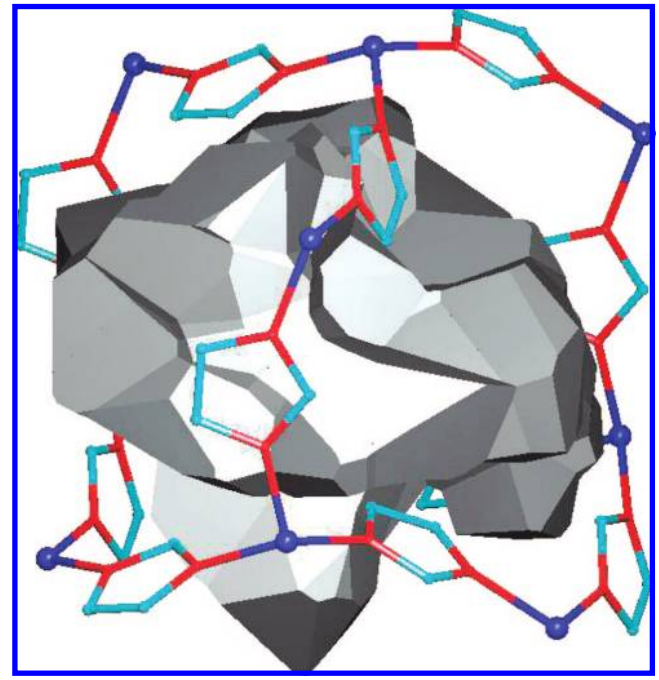

Figure 2. Cavity polyhedron resulting from the fusion of convex Voronoi polyhedra in the diamondoid (**dia**) zinc imidazolate. H atoms are not shown for clarity.

The choice of framework types included in our study resulted from a systematic analysis of nets known to date (from different enumeration techniques[20,22]) and from data on the occurrence of framework types in experimentally characterized MOFs.[6] We concentrate on simplest, *uninodal* frameworks that preferentially occur in MOFs.[6] Nets with the *genera* (that measure network complexity, *cf. below*) in the range 3−25 were chosen, in order to sample configurational space from the simplest to the more complex structures. In ZIFs based on uninodal nets, all zinc atoms are topologically equivalent and, therefore, have identical neighborhoods and coordination spheres. Besides the 6 polymorphs known from experiments, 19 other model polymorphs could be constructed along this line. In addition, we have also included two *binodal* nets, namely, coesite (**coe**) and **cfc** (4-layered carbon allotrope).

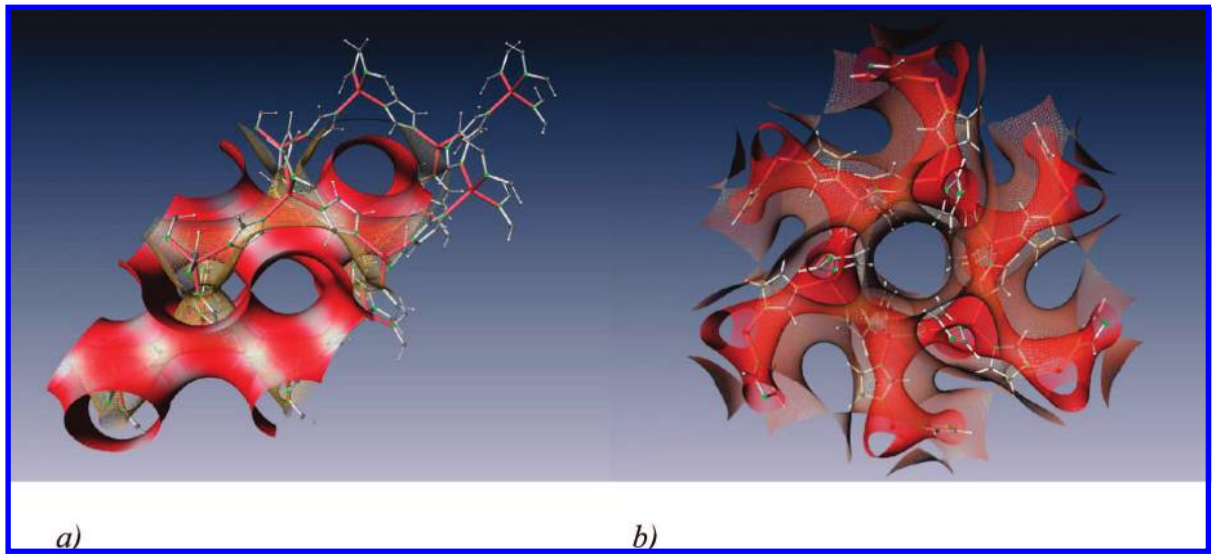

Figure 3. Zinc imidazolates with **dia** (a) and **lcs** (b) topology. A periodic nodal surface, PNS, is represented to stress the topological difference between the nets and to clearly separate the network space from the cavity space. Zn atoms are red; network bonds are white, and N atoms are green. Notice the orientation of the H atoms in the direction of the cavities, more pronounced in the **lcs** network. The **dia** network is viewed along [110]; the **lcs** network is oriented along [111]. Hexagonal loops are visible in the latter, as well as the chirality of the shape.

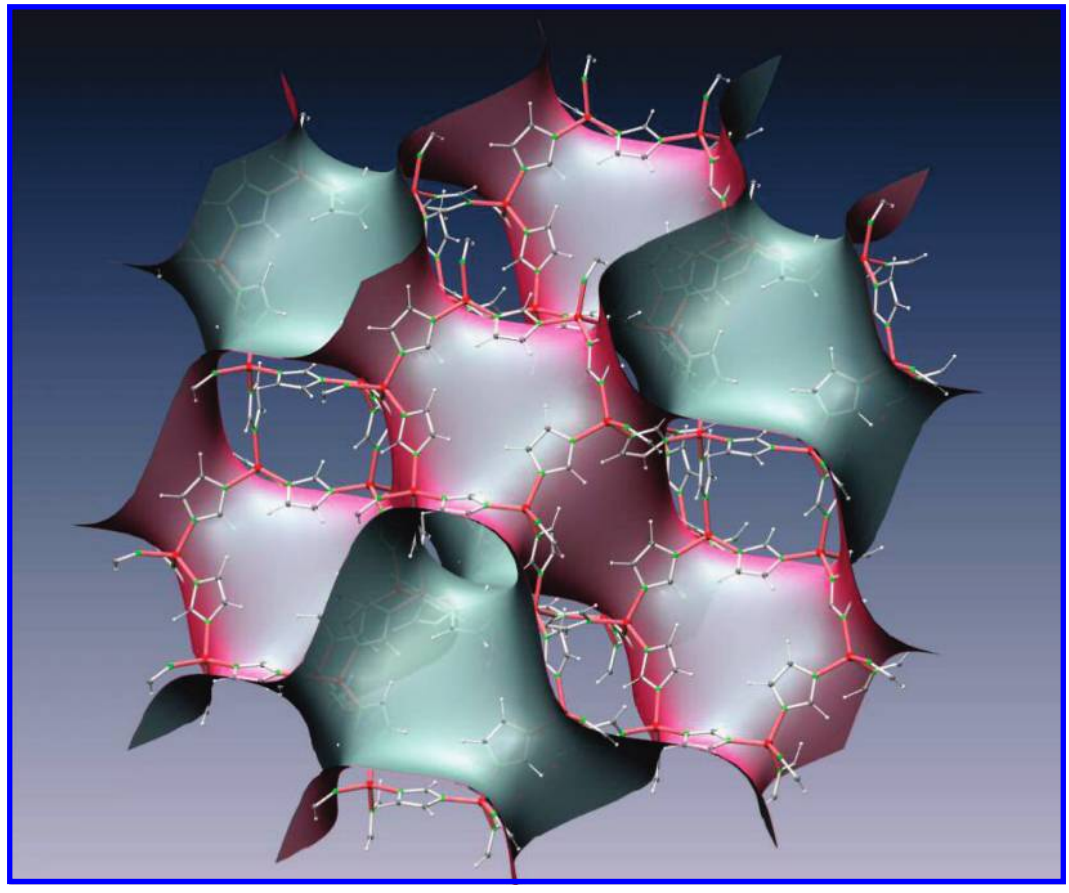

Figure 4. Zinc imidazolate of **sod** topology. A periodic nodal surface, PNS, is represented to highlight the topology and to clearly separate the network space from the cavity space. Zn atoms are red; network bonds are white, and N atoms are green.

Ideal tetrahedral nets in their highest symmetry embedding served as prototypes for constructing ZIFs. Nodes were substituted with metal centers, and the resulting networks were blown up to Zn−Zn spacings in the order of experimental values. An imidazole (IM) molecule was then incorporated with an M−IM−M angle of about 145°. Its initial orientation was chosen based on geometric criteria of nonintersection with other structure parts. The symmetry of the highest embedding was used to replicate the molecule and connect all Zn atoms. In case of restrictions (diamond net, **dia**) imposed by the ligand point group (the highest possible one is *mm*2) on the net space group, the next possible subgroup was used instead.

To properly treat the degree of freedom introduced by the molecular linkers, damped Parrinello−Rahman (dPR) structure optimization was performed, followed by conjugated gradient (CG) structure optimization. The simulation box was chosen to

TABLE 1: Total Energies Per Formula Unit, Energy Differences and Porosity Descriptors for Experimental and Candidate Zinc Imidazolates, Zn(imid)$_2$[a]

structure type	Energy (eV/Zn(imid)$_2$)	difference (with respect to **zni_exp**)	symmetry	packing index, %	solvent accessible volume, %
zni_exp	−3761.0871	0.0000	$I4_1cd$ ($I4_1/acd$)	68.0	7.7
neb	−3760.8249	0.2622	$Fdd2$ ($Fddd$)	57.1	28.3
coe	−3760.8088	0.2783	$P\bar{1}$ ($C2/c$)	58.2	24.5
cag_exp	−3760.7415	0.3456	$Pbca$ ($Cmca$)	52.5	30.2
unj	−3760.6652	0.4219	$P2_1$ ($P6_122$)	49.2	38.3
sod	−3760.6414	0.4457	$R3m$ ($Im\bar{3}m$)	34.1	58.3
mer_exp	−3760.6374	0.4497	$I4/mmm$ ($I4/mmm$)	31.7	61.7
pcb	−3760.6333	0.4538	$Immm$ ($Im\bar{3}m$)	33.0	60.2
gis_exp	−3760.6314	0.4557	$I4_1/amd$ ($I4_1/amd$)	32.1	61.4
lcs	−3760.6312	0.4559	$Ia\bar{3}d$ ($Ia\bar{3}d$)	44.9	45.3
gsi	−3760.6298	0.4573	$P1$ ($Ia\bar{3}$)	55.3	27.9
uni	−3760.6142	0.4729	$P2_1$ ($P6_122$)	48.3	36.4
sra	−3760.6123	0.4748	$C2/c$ ($Imma$)	35.9	57.7
dft_exp	−3760.6047	0.4824	$P4_2/mnm$ ($P4_2/mmc$)	37.0	55.0
dia	−3760.6004	0.4867	Cc ($Fd\bar{3}m$)	43.4	47.3
cfc	−3760.5839	0.5032	$P2_1$ ($P6_3/mmc$)	43.4	47.1
mmt	−3760.5620	0.5251	$P2_12_12$ ($Pccn$)	47.4	41.0
lon	−3760.5603	0.5268	$P2_1$ ($P6_3/mmc$)	43.0	47.7
unc	−3760.5561	0.5310	$P2_1$ ($P4_122$)	46.9	39.9
pcl	−3760.5508	0.5363	$C222_1$ ($Cmcm$)	34.6	58.6
crb_exp	−3760.5177	0.5694	$Pbca$ ($I4/mmm$)	39.2	53.7
irl	−3760.5099	0.5772	Cc ($Ccca$)	42.9	47.7
lta	−3760.4210	0.6661	$P\bar{4}3m$ ($Pm\bar{3}m$)	27.4	67.3
afw	−3760.3621	0.725	$R3$ ($R32$)	36.8	57.0
unh	−3760.4017	0.6854	$P6_1$ ($P6_122$)	47.5	43.3
uoc	−3760.2262	0.8609	$C2$ ($I4_122$)	38.5	55.1
qtz	−3759.9546	1.1325	$P2$ ($P6_222$)	42.5	50.9

[a] Energy differences with respect to the ground state (**zni** structure) are given in a separate column. The MOF symmetry and the maximal possible symmetry of a structure type (given in parentheses) are compared in the column "Symmetry". The packing index is calculated as the ratio of atomic van-der-Waals volumes to unit-cell volume. The solvent accessible volume is derived from tiling the unit cell with van-der-Waals spheres. The net codes of the experimental structures are augmented by the extension *exp*.

include the primitive cell of the ZIFs nets. Separate dPR runs were performed, with and without restrictions on the final lattice type. Typically, imposing constraints on the lattice type ensured a better converge to a lower energy. The lattice type of the maximal symmetry embedding of a net (preserving topology) served as a reference. A Nose thermostat was coupled to the system in the dPR runs, and the geometry relaxed to residual forces smaller than 0.03 eV/Å from high temperature (1000 K) down to the athermal limit (0 K, 0 GPa), with a stress tolerance less than 0.2 GPa. The calculations were performed with the MD facilities of the SIESTA package.[14] Convergence of total energy with respect to number of *k*-points was carefully checked. Calculations including only the origin of the Brillouin zone (Γ-point) with an energy cutoff of 250 Ry ensured convergence of the electronic part for all structures. The calculations were performed within the DFT GGA approximation. The parametrization of Perdew−Burke−Ernzerhof[15] of the exchange-correlation functional was used, together with norm-conserving Trouiller−Martins pseudopontentials. A double-ζ basis set with polarization functions was used on all atoms.

The optimized structures were characterized with respect to porosity and topological density. Porosity was estimated by combining the tiling approach to the description of crystal structures[16] and the Voronoi approach,[17] as implemented in the TOPOS package (http://www.topos.ssu.samara.ru/). In addition, the degree of space filling has also been calculated with traditional "grid" methods based on van der Waals radii as implemented in the PLATON package.[18] Accordingly, a crystal structure can be tiled by means of convex polyhedra (very much like diamond can be divided into adamantane polyhedra, or NaCl into cubes), whereby polyhedral faces are placed halfway between atom centers. The vertices of the convex polyhedra obtained in this way represent voids in a structure. To each void position (polyhedral vertex), a volume can in turn be assigned. In the case of porous structures, the volume contribution of contiguous voids can be summed up. The shape obtained by combining convex, void-centered polyhedra represents the size of the cavity (Figure 2). Its volume is a measure of porosity, while its surface is a first approximation of the internal cavity surface, accessible to solvents or guest molecules. For direct comparison with porosity estimates based on fitting possibly largest spheres in the MOFs scaffoldings based on van der Waals radii, the radius of a sphere of the same volume as the one obtained by Voronoi tessellation can be easily calculated.

The topological density of a framework measures the accumulation of vertices around a reference point. Its numerical value can be expressed as the sum over Zn atoms in the coordination shells of a reference atom.[19] For uninodal networks, only one atom needs to be considered while for binodal nets a weighted sum over two atoms has to be taken. The calculated topological density of the diamond (**dia**) net over 10 coordination shells, TD_{10} is accordingly $1 + 4 + 12 + 24 + 42 + 64 + 92 + 124 + 162 + 204 + 252 = 981$ (1 is added to take into account the central atom).

The *genus* measures the complexity of a network and its degree of connectedness. It can be explicitly calculated for each net on the basis of the Euler relationship, $g = 1 + \epsilon - \nu$, where ϵ is the number of edges and ν is the number of vertices in the primitive cell of a net. For 4-connected nets, the Euler relation reads $g = 1 + 2\nu - \nu = 1 + \nu$. Since the genus is an extensive quantity, its measure is determined with respect to the primitive cell of the net embedding with the highest symmetry. By construction (*cf. above*),

TABLE 2: Structure Types, Physical and Topological Densities, Cavity Radius, and Network Genus for Experimental and Candidate Zinc Imidazolates, Zn(imid)$_2$

structure type	density, g/cm^3	maximal cavity radius, Å	tiling[a]	topological density	genus[b]
zni_exp	1.630	3.90	$[4^2 6^2]$ +2$[6^3 12^2]$	1478	17
neb	1.364	3.60	6^6	1199	5
coe	1.392	3.87	3$[4.9^2]$+$[4.6^2.9^2.10^2]$	1318	9
cag_exp	1.253	5.21	$4^2 6^8$	969	9
unj	1.175	5.29	$5^2 8^2$	1089	7
sod	0.814	6.90	$4^6 6^8$	791	7
mer_exp	0.757	9.32	2$[4^2 8^4]$+$[4^8 8^2]$+$[4^{12} 8^6]$	738	17
pcb	0.787	5.94	$[4^6]$+3$[4^2 8^4]$	787	9
gis_exp	0.766	6.78	$4^6 8^4$	726	9
lcs	1.073	4.54	6^5	1161	13
gsi	1.325	5.23	6^6	1166	9
uni	1.153	4.98	$[6^3]$+$[6.8^2]$	1073	7
sra	0.855	5.64	$4^2 6^2 8^2$	833	5
dft_exp	0.883	5.08	$[4^2 6^2]$+$[6^2 8^2]$+$[4^2 8^4]$	840	9
dia	1.035	4.42	6^4	981	3
cfc	1.035	4.11	$[6^3]$+2$[6^4]$+$[6^5]$	1025	9
mmt	1.134	4.84	6^6	1193	9
lon	1.027	4.36	$[6^3]$+$[6^5]$	1027	5
unc	1.120	4.81	$[6^3]$+$[6.8^2]$	1125	5
pcl	0.825	7.12	$4^4 6^4 8^2$	864	9
crb_exp	0.935	4.54	2$[6^2 8^2]$+$[4^2 6^4]$	959	5
irl	1.026	4.10	$[4^2 10^2]$+$[6^2 10^2]$	962	5
lta	0.654	10.80	3$[4^6]$+$[4^6 6^8]$+$[4^{12} 6^8 8^6]$	641	25
afw	0.878	5.51	$3^2 7^6$	979	4
unh	1.140	6.47	$5^2 12^2$	1029	7
uoc	0.920	4.34	4.8^3	1039	5
qtz	1.023	4.17	$6^2 8^2$	1231	4

[a] Face symbols for polyhedral tiles:[16] the numbers designate n-gonal faces, superscripts refer to the number of n-gonal faces. If there are two or more kinds of tiles, each one is specified in square brackets together with the numbers indicating relative proportion of different tiles. [b] The genera values always refer to the primitive unit cells of ZIFs and are equal to those in the maximal symmetry embeddings of corresponding nets (cf. text).

TABLE 3: Zn−N Distance and Valence Angle Distribution in Experimental and Candidate Zinc Imidazolates, Zn(imid)$_2$

structure type	Zn−N distance, Å	Angle N−Zn−N, degrees
zni_exp	1.96−1.99	101.44−118.34
neb	1.96−2.00	103.51−117.35
coe	1.96−2.00	97.35−125.37
cag_exp	1.95−1.99	103.89−115.85
unj	1.95−2.00	99.00−120.80
sod	1.96−1.97	106.98−112.75
mer_exp	1.96−1.98	104.06−116.41
pcb	1.96−1.99	100.69−125.25
gis_exp	1.96−1.97	103.77−114.62
lcs	1.96−1.97	103.62−113.51
gsi	1.94−2.01	94.43−131.75
uni	1.96−2.01	100.18−119.31
sra	1.96−1.99	99.70−126.46
dft_exp	1.96−1.97	106.36−112.61
dia	1.96−1.98	102.99−118.33
cfc	1.96−1.99	98.88−120.64
mmt	1.97−1.99	98.08−134.30
lon	1.96−2.00	99.92−119.95
unc	1.95−1.99	98.00−127.83
pcl	1.96−2.00	97.55−124.48
crb_exp	1.96−1.99	104.19−115.77
irl	1.96−2.00	96.61−130.14
lta	1.96−2.00	99.48−128.56
afw	1.97−2.00	99.60−127.20
unh	1.98−2.02	98.84−128.01
uoc	1.96−2.03	92.34−154.67
qtz	1.98−2.06	87.56−131.02

the genera of all ZIF nets considered are equal to those in the highest symmetry embedding. The minimal possible genus for 3-periodic nets is 3. There are exactly two 4-connected nets with this property: diamond and the **cds** net.[20] Although the former is the most common tetrahedral net, the latter is preferable for square-like coordination of connectors[21] and was not included into our study. In the RCSR database (Reticular Chemistry Structure Resource, http://rcsr.anu.edu.au), four uninodal 4-connected nets with genus $g = 4$: **afw**, **qtz, nbo, qzd** can be found. We included only **afw** and **qtz** into our enumeration since **nbo** and **qzd** do not allow for tetrahedral nodes.[21] It should be noted that a complete combinatorial enumeration of all 4-connected nets with a given genus has not been done up to now. As is common for enumeration techniques, the number of possible topologies grows extremely fast as the genus is increased.[20,22] Nonetheless, the genus is a sensitive measure of network complexity, and we use it accordingly in this work.

Results

Geometrical Characteristics of the Polymorphs. The relaxed networks were analyzed with respect to their geometrical features. With respect to the starting configurations, the ligands are moderately reoriented, with a tendency of placing hydrogen atoms in the channel scaffoldings of the networks (Figures 3 and 4). The Zn positions are on the contrary less sensitive to relaxation. No unstable network resulted, with respect to optimization; that is, framework topology was conserved in all the cases. All of the polymorphs show similar stereochemical features: Zn−N distances were found to vary around 2.00 Å in the narrow range 1.94−2.06 Å (Table 3, second column). The valence angles (N−Zn−N) show small deviations from the ideal tetrahedral value 109.47 (Table 3, third column). The putative structures allow for a broader value distribution, reflecting the incorporation of untypical structures, while the average values are comparable.

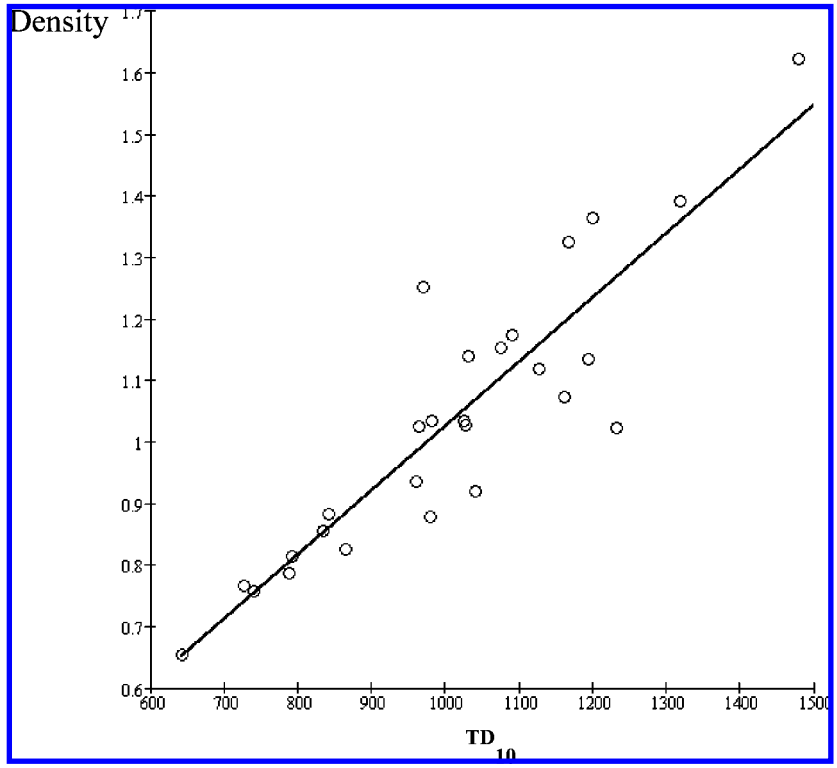

Figure 5. Physical density vs topological density (TD_{10}). A linear correlation can be recognized within a correlation factor of 0.898. The topological density TD_{10} is calculated by summation of the number of atoms in the first 10 coordination spheres around a reference atom.

Upon relaxation the symmetries of the experimental ZIFs are recovered, while for most hypothetical nets a symmetry lower than the maximal embedding is found (Table 1, fourth column). **lcs** on the contrary allows for a cubic symmetry as high as the underlying net. Acentric space groups are the consequence of a missing inversion center on the IM spacers.

DFT Calculations. Total energies corresponding to optimized geometries for the 27 nets considered are listed in Table 1. Therein, the compact structure of the experimentally solvent free zinc imidazolate **zni** sticks out and clearly represents the ground state, lying distinctly below the next best structure, **neb**, which has been observed in $Co(imid)_2$.[23] The latter shares with **zni**, **coe**, and the experimental **cag** network a quite compact atomic arrangement, with low porosity and high packing index (Table 1). In an intermediate energy region, within an energy window of 0.041 eV/formula unit (from **sod** to **dia**), many putative ZIF structures are found among experimental zeolitic ZIF structures. Sodalite (**sod**) is lying lower in energy than the experimentally characterized networks of **mer** and **gis**. The sodalite network was observed in copper imidazolate $Cu(imid)_2$,[24] zinc methylimidazolate,[25] and zinc benzimidazolate.[7] Thus, a sodalite network $Zn(imid)_2$ appears as a reliable candidate. Among the most interesting representative, the diamond network (**dia**), the **pcb**, and the **lcs** networks are found. A diamond network was observed in the structure of $Cd(imid)_2$ that consists of the two interpenetrating **dia** nets.[23] A ZIF based on a single diamond net ($Zn(purine)_2$) has only recently been obtained[26] despite the fact that the **dia** topology is statistically emergent if the totality of known MOFs is considered.[6] Recently,[27] a ZIF with **lcs** topology has been synthesized, using a substituted IM, dichloroimidazole as spacer. Its symmetry is nonetheless identical to the one we are predicting here, that is, $Ia\bar{3}d$. For **pcb**, no candidates have been reported to the best of our knowledge, up to now. Both **pcb** and **lcs** nets represent relatively rare structure types (three experimentally characterized MOF structures have **pcb** topology and only two have **lcs** topology versus more than 200 diamondoid MOFs[6]), despite their inherent cubic symmetry. The least stable network is the ZIF structure based on the quartz net, **qtz**. The disfavor of the latter can be argued from the distortion of the N tetrahedron around Zn (Table 3). Interestingly, this marks a significant deviation from the silica system, where the quartz topology characterizes the ground state and is also present in high-temperature polymorphs (α, β forms of quartz). This underlies the necessity of including energetic arguments besides topological enumeration to properly weight many-body effects, elusive to geometry-based approaches.

Structure Type Versus Network Density. Topological and physical densities (Table 2) correlate almost linearly, with a correlation coefficient of 0.898 (Figure 5). The least topologically dense structures are **gis**, **mer**, **pcb**, **sod**, and **lta**. The latter are also the most porous structures considered and have the lowest physical density. Indirectly, topological density is thus an indication of porosity as it reflects vertex accumulation with the largest ring and cavities. The densest structure shows an unusual **zni** topology and is dense in the topological and the "physical" sense. The lowest energetic ranking indicates **zni**, besides **neb** and **coe** as "molecular crystal", whereby, starting with **sod**, proper framework MOFs start appearing.

Structure Type Versus Porosity. The cavity radii do vary in the range 3.60−10.80 Å. The least porous structures have **neb, zni**, and **coe** topologies and indeed feature dense frameworks. The four most porous structures correspond to the **mer**, **pcl, sod**, and **lta** topologies. This correlates with the reduced topological densities of these framework types. Interestingly, the total energy values for porous structures are distributed in a narrow energy range.

Discussion

The combination of energy ranking and topological enumeration, referring to controlling parameters of network complexity like genus or topological density, is unique in suggesting ZIF candidates that can be considered for synthesis. Compared with enumerations based on packing or geometrical recipes, the optimized structures do reproduce many of the stereochemical features pointed out as optimal for the realization of ZIF networks, like bond length, angle distribution, tetrahedral arrangements around zinc atoms, and valence angles. Nonetheless, the inclusion of total energy evaluations at the DFT level allows capturing an additional aspect of network organization in ZIF compounds. Along the working hypothesis of the strict analogy of tetrahedral networks in terms of realization of similar structural motifs across different systems, the quartz structure for example results as the most unfavorable for a ZIF system. In silicas, the latter represent on the contrary the ground state. Furthermore, in the region where the most porous ZIFs known to date are accumulating, many candidates can be identified, like **sod**, **pcb**, or **gsi**.

As an additional merit of the inclusion of energetic considerations there is the identification of the chiral network **lcs** as good ZIF candidate. With respect to porosity, the **lcs** network is not outstanding. More interesting however is the feature of its intrinsic chiral cavities, which represents a new form of ZIF. Especially, with respect to selective calalysis, this ZIF represents an interesting sample. The occurrence of this topology is quite rare in nature. It is nonetheless found[28] for example in the MOF-like crystal structure of $[Cu_2(scp)_2]\cdot H_2O$ [scp = anion of *N*-(2-hydroxybenzyl)-1-aminocyclopentyl-1-carboxylic acid]. The chirality in the **lcs** ZIF is not enforced by any of its components. It is pertinent to the way spacers and connectors are arranged in space instead. For $[Cu_2(scp)_2]\cdot H_2O$, it is a recrystallization process that it responsible for the formation of the chiral structure from the thermodynamically stable compounds. For ZIF based on **lcs** topology, we expect the use of structure-directing agents, like chiral solvents, or (asymmetric) substitution on the imidazolate spacers to favor the formation of a chiral ZIF. The latter has recently been shown to be a possible strategy.[27]

Finally, the diamond network is found as candidate for ZIF, scoring energetically as well as the experimental **dft** ZIF. Statistically, the diamond topology is well-represented, and it is quite puzzling that it is not common in ZIFs.

The energetic score provided by DFT on ZIFs derived from topology enumeration enlighten the kinetic control of reaction conditions on reaction outcomes. Its merit is to suggest overseen or not-yet synthesized topologies to be realized in the ZIF systems. Clearly, the inclusion of solvents, ionic strength, and free energy considerations are expected to provide a refined picture on how to access some peculiar topologies. Nonetheless, the proper qualification of geometry optimized local minima on the basis of total energy considerations is powerful in shedding light on a variety of shapes that await their experimental realization. In the unique combination with exhaustive topological enumeration, energy scoring is intended as a blueprint for ZIF and in general MOF material design.

Conclusions

In this work, we studied 27 tetrahedral frameworks of zinc imidazolate, ZIFs. Besides polymorphs already characterized, we investigated a wide range of model structures that are distinguished by a different ring statistics or become different in the far coordination spheres. The results show that many structures (**sod**, **pcb**) are energetically very close to porous zeolitic ZIFs known to date, like **mer** or **gis**. DFT total energies clearly isolate a region of accumulation of open-framework structures in a narrow energetic window of strict polymorphism. The correlation between topological density, physical density, and porosity is illustrated. Frameworks with small topological densities are usually the most open structures. However, some of framework types show rather unusual topologies and still represent challenges for synthetic chemists. Therefore, topological modeling and subsequent calculations at the DFT level are a powerful combination for broadening our knowledge of not-yet-synthesized ZIF compounds, and MOFs in general.

Acknowledgment. I.A.B. thanks the "International Max Planck Research School "Dynamical Processes in Atoms, Molecules and Solids" for financial support. We wish to thank Davide Proserpio and Vladislav Blatov for comments on the manuscript. Computational time at ZIH, Dresden is gratefully acknowledged.

Supporting Information Available: Coordinates for all structures in the form of CIF files. This material is available free of charge via the Internet at http://pubs.acs.org.

References and Notes

(1) Kaskel, S., *"Porous Metal-Organic Frameworks" in Handbook of Porous Solids;* Schüth, F., Sing, K. S. W., Weitkamp, J., Eds.; Wiley-VCH: Weinheim, 2002; *Vol. 2*, 1190−1249.
(2) Kitagawa, S.; Kitaura, R.; Noro, S.-I. *Angew. Chem., Int. Ed.* **2004**, *43*, 2334–2375.
(3) Zhao, X.; Xiao, B.; Fletcher. A. J.; Thomas, K. M.; Bradshaw, D.; Rosseinsky, M. J. *Science* **2004**, *306*, 1012–1015.
(4) Férey, G.; Latroche, M.; Serre, C.; Millange, F.; Loiseau, T.; Percheron-Guégan, A. *Chem. Commun.* **2003**, 2976–2977.
(5) Eddaoudi, M.; Kim, J.; Rosi, N.; Vodak, D.; Wachter, J.; O'Keeffe, M.; Yaghi, O. M. *Science* **2002**, *295*, 469–472.
(6) Ockwig, N. W.; Delgado-Friedrichs, O.; O'Keeffe, M.; Yaghi, O. M. *Acc. Chem. Res.* **2005**, *38*, 176–182.
(7) Park, K.; Ni, Z.; Cote, A. P.; Choi, J.-T.; Uribe-Romo, J.; Chae, H. K.; Huang, R.; O'Keeffe, M.; Yaghi, O. M. *Proc. Natl. Acad. Sci. U.S.A.* **2006**, *103*, 10186–10191.
(8) Mattesini, M.; Soler, J. M.; Yndurain, F. *Phys. Rev. B: Condens. Matter* **2006**, *73*, 94111−194111−8.
(9) Tafipolsky, M.; Amirjalayer, S.; Schmid, R. *J. Comput. Chem.* **2007**, *28*, 1169.
(10) Kuc, A.; Enyashin, A.; Seifert. G, *J. Phys. Chem. B* **2007**, *111*, 8179–8186.
(11) Rosi, N. L.; Eddaoudi, M.; Kim, J.; O'Keeffe, M.; Yaghi, O. M. *Cryst. Eng. Commun.* **2002**, *4*, 401–404.
(12) Lehnert, R.; Seel, F. *Z. Anorg. Allg. Chem.* **1980**, *464*, 187–194.
(13) Delgado-Friedrichs, O.; O'Keeffe, M. *J. Solid State Chem.* **178**, 2480–2485.
(14) Soler, J. M.; Artacho, E.; Gale, J. D.; García, A.; Junquera, J.; Ordejón, P.; Sánchez-Portal, D. *J. Phys.: Condens. Matter* **2002**, *14*, 2745–2779.
(15) Perdew, J. P.; Burke, K.; Ernzerhof, M. *Phys. Rev. Lett.* **1996**, *77*, 3865.
(16) Blatov, V. A.; Delgado-Friedrichs, O.; O'Keeffe, M.; Proserpio, D. M. *Acta Crystallogr., Sect. A* **2007**, *63*, 418–425.
(17) Blatov, V. A.; Shevchenko, A. P. *Acta Crystallogr., Sect. A* **2003**, *59*, 34–44.
(18) Spek, A. L. *J. Appl. Crystallogr.* **2003**, *36*, 7–13.
(19) O'Keeffe, M. *Z. Kristallogr.* **1991**, *196*, 21–37.
(20) Beukemann, A.; Klee, W. E. *Z. Kristallogr.* **1992**, *201*, 37–51.
(21) Delgado-Friedrichs, O.; O'Keeffe, M.; Yaghi, O. M. *Phys. Chem. Chem. Phys.* **2007**, *9*, 1035–1043.
(22) Treacy, M. M. J.; Randall, K. H.; Rao, S.; Perry, J. A.; Chadi, D. A. *Z. Kristallogr.* **1997**, *212*, 768–791.
(23) Yun-Qi, Tian.; Chen-Xin, Cai.; Xiao-Ming, Ren.; Chun-Ying, Duan.; Yan Xu, Song Gao.; Xiao-Zeng, You. *Chem. Eur. J.* **2004**, *9*, 5673–5685.
(24) Masciocchi, N.; Bruni, S.; Cariati, E.; Cariati, F.; Galli, S.; Sironi, A. *Inorg. Chem.* **2001**, *40*, 5897–5905.
(25) Yun-Qi, Tian.; Chen-Xin, Cai.; Yong, Ji.; Xiao-Zeng, You.; Shie-Ming, Peng.; Gene-Hsiang, Lee. *Angew. Chem., Int. Ed.* **2002**, *41*, 1384–1386.
(26) Hayashi, H.; Cote, A. P.; Furukawa, H.; O'Keeffe, M.; Yaghi, O. *Nature Mater.* **2007**, *6*, 501–506.
(27) Banerjee, R.; Phan, A.; Wang, B.; Knobler, C.; Fukurawa, H.; O'Keeffe, M.; Yaghi, O. M. *Science* **2008**, *319*, 939–943.
(28) Sreenivasulu, B.; Vittal, J. J. *Cryst. Growth Des.* **2003**, *3*, 635–637.

JP801681W